IIETA International Information and Engineering Technology Association
Advancing the World of Information and Engineering

Revue des Composites et des Matériaux Avancés-Journal of Composite and Advanced Materials
Vol. 35, No. 2, April, 2025, pp. 281-293
Journal homepage: http://iieta.org/journals/rcma

Impact of Sintering Duration on the Mechanical and Bioactive Properties of Pure Ti, Ti-Al Alloy, and Ti-Al-HAp Composite for Biomedical Applications

Marwa H. Hadi*, Niveen J. Abdulkader, Layth W. Al-Gebory

Department of Materials Engineering, University of Technology - Iraq, Baghdad 10069, Iraq

Corresponding Author Email: mae.22.040@grad.uotechnology.edu.iq

Copyright: ©2025 The authors. This article is published by IIETA and is licensed under the CC BY 4.0 license (http://creativecommons.org/licenses/by/4.0/).

https://doi.org/10.18280/rcma.350210

Received: 27 February 2025
Revised: 31 March 2025
Accepted: 12 April 2025
Available online: 30 April 2025

Keywords:
MTT, relative density, biomaterials, hydroxyapatite, biocompatibility, powder metallurgy, titanium

ABSTRACT

Commercially pure titanium is widely used in biomedical applications due to its excellent biocompatibility, although its bioinert nature limits osseointegration. This study incorporated hydroxyapatite (HAp) to enhance bioactivity, and aluminum (Al) was added to improve mechanical performance. The effect of sintering time on the relative density, compressive strength, microhardness, and bioactivity of CP-Ti, Ti–6%Al, and Ti–6%Al–2%HAp composites was investigated. The samples were fabricated via powder metallurgy and sintered at 1300°C for 60, 90, and 120 minutes. Results indicated that increasing the sintering time improved all evaluated properties. At 120 minutes, relative densities reached 91.72%, 92.78%, and 93.31%, while compressive strengths were 511 MPa, 492 MPa, and 476 MPa for CP-Ti, Ti–6%Al, and Ti–6%Al–2%HAp, respectively. Microhardness values also increased, reaching 379 HV, 351 HV, and 298 HV. XRD analysis identified the formation of bioactive phases, including TiP_2O_7, TiO_2, Al_2Ti, $Na_2Ti_3O_7$, $CaTi_4P_6O_{24}$, and $CaTiO_3$. The MTT assay confirmed low cytotoxicity (13.3%) in three days. AAS results showed minimal Ti (0.912 ppm) ions and no Al ions release in 14 days. These findings highlight the significant role of sintering time in enhancing the mechanical and bioactive performance of Ti-based composites for biomedical applications.

1. INTRODUCTION

Orthopedics, a clinical medicine subdivision, focuses on diagnosing and treating illnesses and injuries of the musculoskeletal system, including extremities and the spine. It has evolved significantly due to advancements in biomaterials science [1]. Metals such as cobalt and titanium-based alloys are favored in orthopedic applications due to their high strength, fracture resistance, and suitable biocompatibility [2, 3]. Commercial pure titanium (CP-Ti) and its alloys are widely used in orthopedic implants in the human body, including dental implants, crowns, bridges, joint replacements, bone fixation plates, and more [4] for their mechanical stability and inertness to biological reactions [5]. CP-Ti and its alloys exhibit excellent biocompatibility, high corrosion resistance to body fluids, and desirable mechanical properties such as a high strength-to-weight ratio [6].

For non-load-bearing applications, titanium and its alloys are recommended for their excellent ability to integrate well with bone tissue without causing significant adverse effects [7]. To meet implants' demanding mechanical and biological requirements, titanium alloys are processed using various techniques, such as powder metallurgy (P/M), casting, cold working, machining, hot working, and additive manufacturing [8]. The two main techniques for manufacturing Ti alloy implants are powder metallurgy and casting [9]. The P/M method, in particular, is favored due to its cost-effectiveness and ability to produce near-net-shape parts with excellent surface quality [10]. This technique has been instrumental in fabricating titanium alloys with optimized properties for biomedical applications [11]. The success of the P/M process (including powder mixing, compacting powder, and the sintering process [12]) depends on thorough characterization and control of the metal powder, including the distribution of particle size, structure, sintered material characteristics, and behaviors during compression and sintering stages [10].

Despite the advantages of titanium and its alloys, challenges remain in optimizing their properties for biomedical applications. The processing conditions, such as sintering temperature and time, as well as the incorporation of other elements like aluminum and hydroxyapatite, significantly influence the material's final properties, including mechanical strength, micro-hardness, and biocompatibility [13]. The sintering temperature directly depends on the melting temperature of the base element (Ti), which is approximately 1678°C [14]. The sintering temperature optimum range is usually limited between 60% to 80% of the melting temperature of the base element, therefore, in this case, the sintering temperature is 1,006°C to 1,342°C. The high sintering temperature led to a closure of the pores and reduced their total number, causing them to be of a spheroidal shape in morphology [15]. Longer sintering times improve

densification but at diminishing rates due to the gradual loss of the driving force for sintering. Extended sintering time offers diminishing benefits after the material reaches a near-equilibrium state [16]. By optimizing these parameters—temperature and time, the sintering process can be tailored to produce materials with specific properties required for biomedical and industrial applications [17].

One challenge in using titanium alloys for biomedical applications is their limited biocompatibility, primarily due to their bioinert nature. The hydroxyapatite (HAp) with the chemical formula of $Ca_{10}(PO_4)_6(OH)_2$ is commonly incorporated into titanium alloys to address this limitation and is the greatest hopeful bio-ceramic material because of its exclusive biocompatibility properties. The presence of Calcium-phosphate ceramic (bioactive oxide) in this material leads to improved bioactivity. The HAp is an outstanding bioactive agent transporter for the growth of tissue due to its composition similar to that of natural bone [18]. The HAp incorporation provides the calcium (Ca) and phosphorus (P) distribution, which could aid better bone osseointegration than implants made of pure metal alloys. Combining Ti alloys with HAp ceramic creates a unique bio-material with excellent biological and mechanical properties [19]. Moreover, adding aluminum (Al) to titanium further enhances its mechanical properties, such as tensile strength, hardness, and fatigue resistance, making it more suitable for high-stress applications like joint replacements and bone fixation. The addition of aluminum also helps to improve the material's resistance to wear and corrosion, which are critical factors in the longevity and reliability of implants. This makes titanium-aluminum alloys highly desirable for use in the medical field, especially for load-bearing implants [20].

Omidi et al. [21] utilized spark plasma sintering (SPS) to fabricate titanium-hydroxyapatite (HAp) composites with varying HAp content (0%-40%) in multiple layers. They observed an increase in grain size and an initial rise in Vickers microhardness, which decreased at higher HAp content. The maximum compressive strength was achieved with five-layer samples, emphasizing the need to optimize HAp content. However, sintering conditions and the impact of alloying elements like aluminum were not explored, which is a focus of the current study. Kobayashi et al. [22] investigated the biocompatibility of Ti-HAp composites fabricated by compressive shear, using MC3T3-E1 mouse osteoblasts. They found that HAp remained stable at 800°C but decomposed slowly at 1100°C, with higher HAp content reducing cell proliferation. This study provided insights into biocompatibility but did not address the influence of sintering temperature on mechanical properties or the combination of titanium with other elements, a topic covered in the present research [22]. Farrahnoor and Zuhailawati [23] studied Ti-Nb-HAp composites through powder metallurgy, finding that XRD analysis revealed phases like TiO_2 and Ti2P as HAp content increased. Maximum bioactivity occurred at 15 wt.% HAp, though sintering conditions were not considered. The current research aims to investigate both the mechanical and biological properties of Ti-based composites under varying sintering conditions.

Shanmuganantha et al. [24] fabricated Ti-HAp and Ti-$CaSiO_3$ composites using hot press compression and vacuum sintering, showing good biocompatibility with human osteoprogenitor cells. While they emphasized bioactivity and titanium strength, the study did not examine the effect of alloying elements like aluminum on mechanical properties, which this research addresses [24]. Arivazhagan et al. [25] developed Ti-6Al-4V implants enhanced with HAp, significantly improving biomechanical and biological performance. While they demonstrated HAp's potential for osseointegration, the study did not explore sintering conditions or alloying elements, which will be investigated in the present work [25]. Sadlik et al. [26] fabricated porous Ti/HAp composites with varying HAp content using powder metallurgy. They observed that introducing HAp decreased microhardness but increased biological activity, though the effects of sintering conditions or alloying elements were not addressed. These aspects will be further explored in this study. Yaşar and Ekmekci [27] studied the effects of micro- and nano-HAp powder sizes on surface topography and biocompatibility of Ti-6Al-4V alloy using Electrical Discharge Machining (EDM). They found that micro-HAp reduced surface roughness and improved wettability, while nano-HAp had minimal effects. However, this study did not investigate bulk mechanical properties, such as hardness and compressive strength, which will be examined in the current research [27]. While studies have examined the interaction of titanium with hydroxyapatite or aluminum separately (e.g., Omidi et al. [21]; Yaşar and Ekmekci [27]), no comprehensive research has investigated the combined effect of all three elements in a single sintering process.

Our study contributes a new perspective by examining the impact of this three-component mixture and provides quantitative evidence of its influence on the mechanical and microstructural properties of the sintered material.

Although previous studies have explored the biocompatibility and mechanical properties of Ti-HAp composites, there is a gap in understanding the combined effects of aluminum and HAp in Ti-based composites, particularly with varying Ti particle sizes. The impact of sintering time on mechanical and biological properties has also not been thoroughly investigated. This study aims to fill these gaps by preparing Ti-based materials (CP-Ti, Ti-6%Al alloys, and Ti-6%Al-2%HAp composites) using powder metallurgy, focusing on optimal sintering times and assessing density, compressive strength, micro-hardness, and biological properties for biomedical applications.

2. EXPERIMENTAL WORK

In this study, titanium powders (Ti1 and Ti2) with two distinct particle sizes, aluminum (Al) powder as the reinforcement constituent, and hydroxyapatite (HAp) nano-powder as the bioactive component were used.

2.1 Work procedure

The powder metallurgy technique was employed to prepare nine samples, categorized into three groups (A, B, and C) based on their composition and sintering time. Each group included three types of samples: (1) pure titanium (100% Ti), (2) a Ti-6%Al alloy, and (3) a Ti-6%Al-2%HAp composite. Two titanium particle sizes (Ti1 and Ti2) were utilized, maintaining a 70% Ti1 to 30% Ti2 ratio across all samples (this bimodal particle size distribution effectively enhanced the packing density of the powder, as smaller particles filled the voids between larger ones, thereby reducing porosity and increasing bulk density) [28].

2.2 Green compact preparation

The samples were prepared using the powder metallurgy technique, which involves mixing, compacting, and sintering. The weighed powders were placed into a securely sealed container and mixed for 4 hours at a constant speed of 100 rpm in air at RT with Ethanol as a binder (A mixing duration ranging from 2 to 6 hours can generally be considered suitable balancing mixing time to avoid particle fracture or cold welding [29] while the powder homogeneity was verified through visual inspection. The uniformity of the mixture was assessed by checking for visible clumps or inconsistencies in color, with the absence of these indicating satisfactory homogenization. After mixing, the rectangular mold cavity (2× 1× 3 cm^3) was gradually filled with the powder. The die was then transferred to a hydraulic press device, where the powders were compacted at 600 MPa for 10 minutes at a speed of 0.5 mm/s (Titanium powder compaction in powder metallurgy requires high pressures, typically ranging from 100 MPa to 1,000 MPa, depending on particle size, shape, and binder content [30]). Additionally, although the current compaction method employed uniaxial pressing, it acknowledges the possibility of density gradients. To minimize this effect, we maintained a consistent compaction pressure and ensured uniform die-filling. Each green compact had been produced with dimensions of 2×1×1 cm^3. Each green compact sample of these groups had its symbol of meeting the research goals (Table 1).

Table 1. Groups of green compact samples.

Group	Sample	Symbol	Sample	Symbol	Sample	Symbol
A	100% Ti	T_A	Ti6%Al	TA_A	Ti6% Al2% HAp	TAH_A
B	100% Ti	T_B	Ti6%Al	TA_B	Ti6% Al2% HAp	TAH_B
C	100% Ti	T_C	Ti6%Al	TA_C	Ti6% Al2% HAp	TAH_C

2.3 Sintering process

The green compacts were categorized into three groups (A, B, and C) for the subsequent powder metallurgy (P/M) sintering process based on the designated sintering times. The samples in Groups A, B, and C were sintered for 60, 90, and 120 minutes at a sintering temperature of 1,300℃. Several studies have demonstrated that sintering commercially pure titanium or Ti-6Al-4V alloys at ~1300℃ for 60–120 minutes under vacuum or inert gas atmospheres achieves near-full densification with minimal grain growth and optimal mechanical performance [31]. Table 2 and Figure 1 depict the samples prepared after sintering at different times in this study.

Table 2. Groups of samples

Sample	Sintering Time (min)
T_A, TA_A, TAH_A	60
T_B, TA_B, TAH_B	90
T_C, TA_C, TAH_C	120

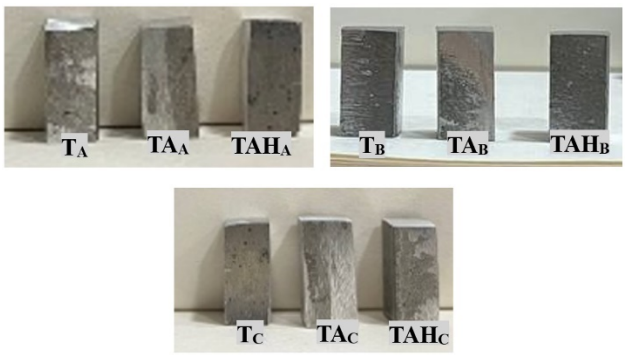

Figure 1. Samples prepared

2.4 Sintering process

The green compacts were categorized into three groups (A, B, and C) for the subsequent powder metallurgy (P/M) sintering process based on the designated sintering times. The samples in Groups A, B, and C were sintered for 60, 90, and 120 minutes at a sintering temperature of 1,300℃. Several studies have demonstrated that sintering commercially pure titanium or Ti-6Al-4V alloys at ~1300℃ for 60–120 minutes under vacuum or inert gas atmospheres achieves near-full densification with minimal grain growth and optimal mechanical performance [31]. Table 2 and Figure 1 depict the samples prepared after sintering at different times in this study.

3. CHARACTERIZATION

3.1 The powder characterization

3.1.1 Chemical composition characterization

Elemental analyses of the powders (Ti1, Ti2, Al, and HAp) were performed by X-ray fluorescence (XRF) analysis using the SPECTRO Analytic Instrument model (XEPOS) at 100 V.

3.1.2 Particle size characterization

The particle sizes of each powder (Ti1, Ti2, Al, and HAp) were measured using a DLS Bookhaven 90Plus Particle- USA Size Analyzer following ASTM B822-20 [32].

3.2 Sample characterization

3.2.1 The density and relative porosity measurements

The apparent density, relative density, and relative porosity of each sample produced after sintering at various sintering times were calculated using the Archimedes method with a density measurement according to ASTM ISO3369:1975 standard procedures. Each sample's dry weight (W_d) was measured. Subsequently, these samples were immersed (saturated) in water for 24 hours, followed by measuring their weight (w_n), and were calculated according to the subsequent rule in Eq. (1) [33]. Three readings were taken for each sample, and the average apparent density was calculated. Additionally, the values were compared with the standard deviation, and the error bar was determined. The theoretical density ($\rho_{theoretical}$) for each specific composition is 4.5 g/cm^3 for 100% Ti, 4.392 g/cm^3 for 94% Ti-6Al, and 4.3648 g/cm^3 for 92% Ti-6% Al-2% HAp. Each sample's relative density ($\rho_{relative}$) was calculated according to Eq. (2) [34]. Finally, the relative porosity of each sample was determined according to Eq. (3) [35].

$$\rho_a = \frac{wd}{wd - wn} * \check{D} \quad (1)$$

$$\rho_{relative} = \frac{\rho a}{\rho theoretical} \quad (2)$$

$$\textbf{Relative Porosity} = \left\{1 - \left(\frac{\rho relative}{\rho theortical}\right)\right\} * 100 \quad (3)$$

where,

ρ_a = the apparent density (g/cm³),
w_d = the dry sample weight (g),
w_n = the immersed test sample weight (g), and
$\check{D}$ = the water density (g/cm³).

3.2.2 Compression tests

The compression strengths of all samples were determined following the ASTM E9 standard using a universal testing machine (Laryee Technology Co. LTD) [36].

3.2.3 Microhardness tests

The microhardness of all samples was measured using a microhardness testing apparatus (LAYREE, Netherlands) following ASTM E18-07. Vickers hardness testing was performed by applying a pyramidal-shaped diamond indenter to the sample surface under a load of 5 N for 15 seconds [37].

3.3 Extra Inspections

The best-performing sample from the tests above was exposed to extra inspections such as XRD, SEM, EDS, AAS, and MTT assay.

3.3.1 X-ray diffraction inspection

The microstructural phases of the best-performing sample in this study were analyzed using X-ray diffraction (XRD). The measurements were performed with a Shimadzu X-Ray Diffractometer (model XRD-6000), which employs a Cu X-ray tube and operates within a 2θ range of -6° to 163°, with an angular resolution of 0.002°.

3.3.2 Morphology inspections

The surface morphologies of the best-performing sample were analyzed using scanning electron microscopy (SEM), while the detailed elemental composition and distribution were determined through energy dispersive X-ray spectroscopy (EDS), both performed using a Thermo Scientific Axia model Scanning Electron Microscope (SEM) made in the Netherlands.

3.3.3 Atomic Absorption Spectroscopy (AAS) characterization

Atomic Absorption Spectroscopy (AAS) was employed to quantify the ions released at three specific time intervals (3, 7, and 14 days) from the best-performing sample in this study. The measurements were performed in Ringer's solution, a fluid formulated to mimic the ionic composition of human body fluids, ensuring physiological relevance in the analysis (the composition of Ringer's solution is shown in Table 3). The sample was immersed in a 100 mL glass beaker containing Ringer's solution, incubated in a water bath at 37°C, and aliquots of the solution were extracted using a syringe at 3, 7, and 14 days. Ion release was monitored throughout the 14-day immersion period. The extracted solutions were analyzed using a novAA 400P atomic absorption spectrometer (Germany). Figure 2 illustrates the procedure of this test [38].

Table 3. Components of Ringer's solution

No.	Component	Concentration (gm./L)
1.	NaCl	8
2.	Glucose	1
3.	KCl	0.4
4.	Na HCO_3	0.35
5.	Na $H_2PO_4.H_2O$	0.25
6.	Ca $Cl_2.2H_2O$	0.19
7.	Mg Cl_2	0.10
8.	Mg $SO_4.7H_2O$	0.06
9.	Na_2 $HPO_4.2H_2O$	0.06

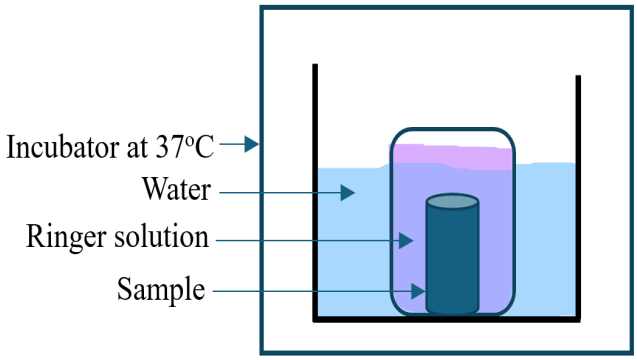

Figure 2. The incubation during the AAS testing process

3.3.4 MTT assay characterization

The MTT assay, a tetrazolium-based method, was employed to evaluate cell viability (%) and cytotoxicity (%) using the Promega GloMax Discover GM3000. MG63 human bone fibroblast cells (10^3 cells/well) were seeded in 100 µL of DMEM, supplemented with Ti-6%Al-2%HAp powder (0.1 ng/mL) in its nanoscale form (nHAp). The cells were incubated at 37°C for 24, 48, and 72 hours, with careful monitoring of incubation conditions to maintain optimal growth, including a consistent 5% CO_2 level to preserve pH balance in the medium. Following the incubation periods, 10 µL of MTT reagent was added to each well and incubated for an additional 4 hours. This reagent is reduced by viable cells to form purple formazan crystals. After incubation, formazan crystals were solubilized by adding 100 µL of DMSO and allowing the reaction to complete at room temperature for 24 hours. The absorbance was then measured at 550 nm using a spectrophotometer to quantify the formazan produced as shown in Figure 3. Control wells (untreated cells) showed approximately 100% viability, and the cell viability of the treated samples was calculated using the following formula [39]:

Cell viability (%) = (Mean absorbance of treated cells / Mean absorbance of control cells)*100%. (4)

In this study, the response of MG63 cells to Ti-6%Al-2%HAp powder was also assessed through the MTT assay. The results of the mitochondrial activity assay demonstrated that the tested sample had no toxic effects on the MG63 cells, with cell viability rates remaining above 70% after incubation for 1, 2, and 3 days. These findings support the biocompatibility of Ti-Al-HAp, confirming its potential as a viable biomaterial for biomedical applications, including implants.

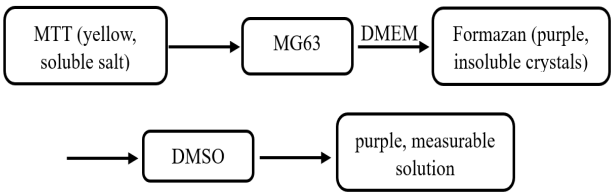

Figure 3. Block diagram of MTT assay

4. STATISTICAL EVALUATION OF MECHANICAL PROPERTIES

The microhardness and apparent density results were analyzed using one-way ANOVA. Data are presented as mean values accompanied by standard deviation and standard error. Statistical analysis was performed using SPSS software (version 22).

5. RESULTS AND DISCUSSION

5.1 Particle size analysis

Figures 4-7 show the examination chart revealed effective diameters of the starting powders, 484.9 nm for Ti1 powder, 174.6 nm for Ti2 powder, 112.5 nm for Al powder, and 72.5 nm for HAp powder, respectively, with minor size variations. Using a combination of coarse and fine particles in sintered materials can significantly impact both compressibility and microhardness. The fine particles fill the voids between the coarse particles, leading to a denser structure that reduces compressibility. This results in a material that is less prone to deformation under pressure.

Additionally, the mixture of particle sizes enhances the bonding between particles during sintering, improving the material's overall hardness. The fine particles contribute to a more uniform distribution of stress, which increases the microhardness by enhancing resistance to scratching and wear. However, an imbalance in the ratio of coarse to fine particles can lead to variability in hardness due to weaker regions in the material [40]. Particle size plays a crucial role in the sintering process. A reduction in particle size enhances the sintering process. Smaller particles possess a larger pore-to-solid interfacial area, which generates a stronger driving force for sintering. This leads to increased diffusion mechanisms. Greater surface area accelerates surface diffusion, finer grain sizes facilitate grain boundary diffusion, and larger interparticle contact areas promote volume diffusion. Table 4 shows the powder properties of each material used in this work.

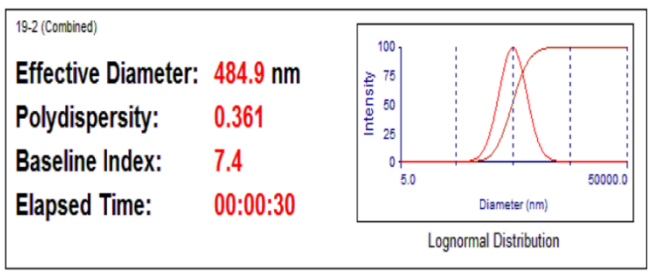

Figure 4. Size distribution of Ti1 powder

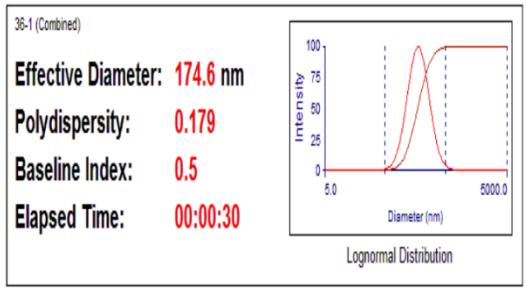

Figure 5. Size distribution of Ti2 powder

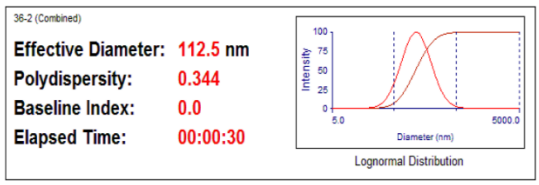

Figure 6. Size distribution of Al powder

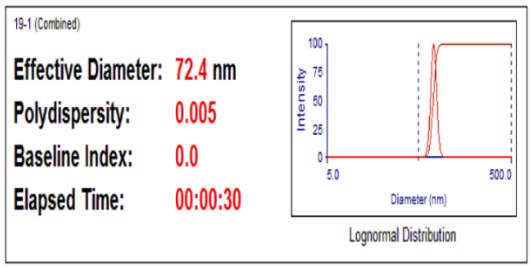

Figure 7. Size distribution of HAp powder

Table 4. Starting powder properties

Component	Particle Size (nm)	Purity (%)
Titanium1 (Ti1)	484	98.81
Titanium2 (Ti2)	174	98.76
Aluminum (Al)	112	98.32
Hydroxyapatite (HAp)	72	95.43

5.2 X-ray fluorescence (XRF) analysis

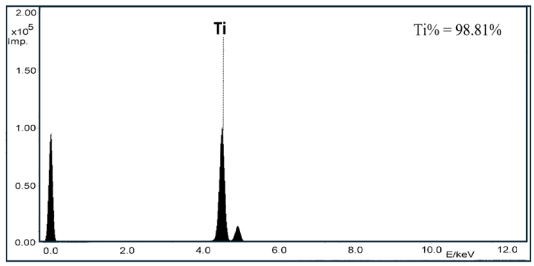

Figure 8. XRF analysis of Ti1 powder

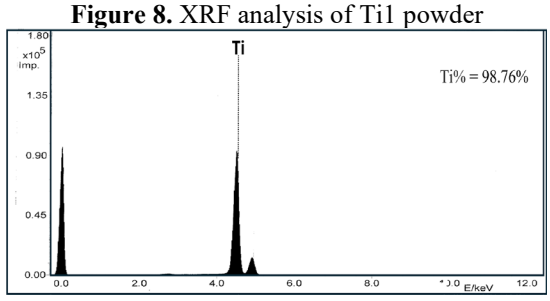

Figure 9. XRF analysis of Ti2 powder

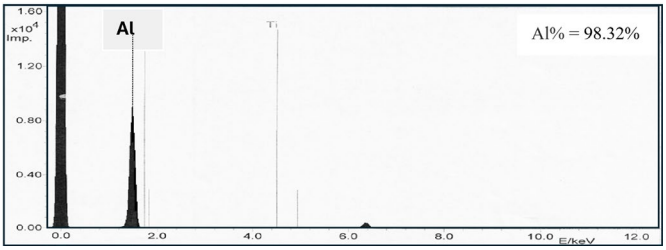

Figure 10. XRF analysis of Al powder

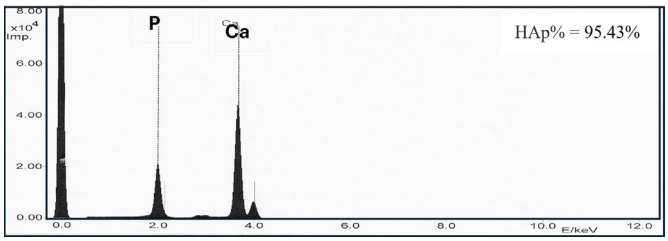

Figure 11. XRF analysis of HAp powder

Figures 8-11 show the chemical analysis results for (Ti1, Ti2, Al, and HAp) powders, respectively. XRF analysis reveals the purity of each powder, along with the elements that appeared as impurities and their respective percentages. This analysis also showed that Ti1 powder, Ti2 powder, Al powder, and Hap powder concentrations reached 98.81%, 98.76%, 98.32%, and 95.43%, respectively**.** This figure shows that the powders used to produce these alloys are pure. The XRF analysis of as-received powders confirms the existence of the essential elements.

5.3 Density and porosity results

Figures 12-14 present the density measurements for the various samples, showing the apparent density (g/cm³), relative density (%), and relative porosity (%) as functions of sintering times (60, 90, and 120 minutes). The data indicate that both apparent and relative densities increase, while relative porosity decreases, with extended sintering times. Specifically, increasing the sintering time from 60 to 120 minutes resulted in significant increases in both apparent and relative densities, accompanied by a decrease in relative porosity. The highest density values for all compositions (group C: T_C, TA_C, and TAH_C) were recorded at a sintering time of 120 minutes. These results highlight the crucial role of prolonged sintering in reducing porosity and enhancing densification.

Among all the samples, TAH_C—sintered at 1,300°C for 120 minutes—exhibited the highest relative density (93.31%) and the lowest relative porosity (0.7862%), with an apparent density of 4.067 g/cm³. Longer sintering times facilitate pore closure, reducing pore number and promoting spheroidal pore structure formation [41]. Furthermore, the incorporation of aluminum (Al = 2.7 g/cm³) and hydroxyapatite (HAp = 3.14 g/cm³) contributes to enhanced densification, bringing the measured densities closer to the theoretical density of titanium (4.5 g/cm³). Notably, aluminum aids in the formation of the α-phase in titanium alloys, which is less dense than the β-phase [42].

The composite samples consist of particles of various sizes: Ti1 (484 nm), Ti2 (174 nm), Al (112 nm), and HAp (72 nm). The moderate porosity observed, which is typical of titanium-based implants, facilitates tissue adhesion while maintaining sufficient mechanical strength. the porosity level also hurts (negative effect) the biomaterial implant's mechanical properties. The porosity presence can reduce the mechanical strength of the biomaterial implant. In the structure of a material, the pores can perform as stress concentrators, which leads to fatigue strength reduction [43].

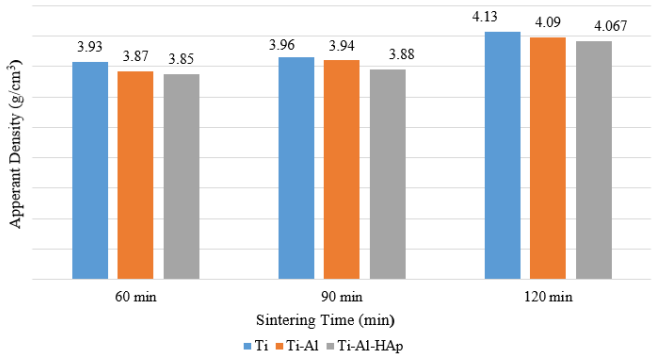

Figure 12. Apparent density – sintering time chart

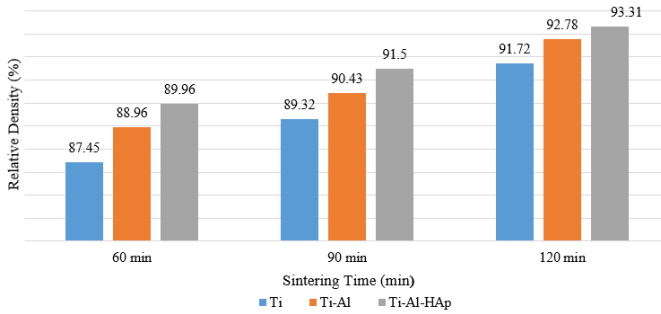

Figure 13. Relative density – sintering time chart

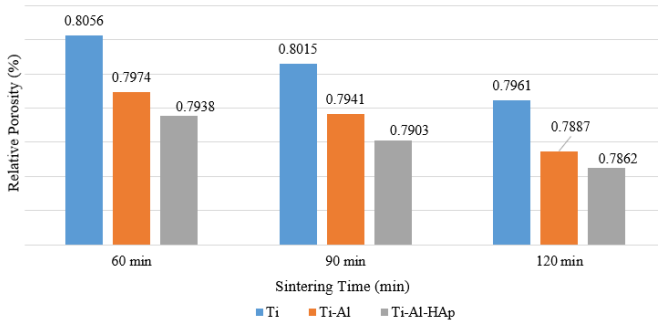

Figure 14. Relative porosity - sintering time chart

This balance is crucial for minimizing adverse biological reactions and promoting healing [44]. Additionally, the relative density of sample TAH_C (93.31%) aligns with typical values reported for titanium-based implants, which range from 85% to 95% [45], while the density of Ti-6Al-4V alloy typically ranges between 4.43 to 4.48 g/cm³ [46].

Hoseinzadeh et al. [47] investigate how varying sintering times affect the microstructure, phase, density, and mechanical and tribological properties of Cf/Si_3N_4 composites. Findings indicate that optimal sintering time enhances densification.

5.4 Compression test results

Figure 15 shows each sample's compressive strength (MPa) as a function of sintering times. The data indicate that the

compressive strength of the samples increases with longer sintering times. Specifically, the compressive strength continues to rise with sintering times of 60, 90, and 120 minutes, reaching its peak at 120 minutes for group C. The maximum compressive strengths of group C (T_C=511 MPa, TA_C=492 MPa, and TAH_C=476 MPa) were achieved under the highest sintering conditions (1,300°C for 120 minutes), which also led to a reduction in porosity, as previously discussed.

The varying particle sizes (Ti1=484 nm, Ti2=174 nm, Al=112 nm, HAp=72 nm) contributed to improved toughness by enhancing phase homogeneity and particle interactions, resulting in increased material strength and resistance to deformation. However, the addition of aluminum (Al) and hydroxyapatite (HAp) to titanium (Ti) led to a decrease in compressive strength, as expected. While pure Ti exhibits high strength, the incorporation of Al alters its microstructure, and HAp, although beneficial for biocompatibility, is brittle and does not significantly contribute to compression strength [48]. The compressive strength of pure Ti typically ranges from 130 to 170 MPa, with some reports indicating values between 240 and 550 MPa depending on factors such as purity and processing conditions. In comparison, the compressive strength of human trabecular bone is between 2 and 80 MPa [49] while the compressive strength of Ti-6Al-4V alloy typically ranges between 1074 to 1661.6 MPa [50]. D. Kumar, E. Zhang, and F. Nguyen focus on the effect of sintering duration on the mechanical strength and bioactivity of Ti-6Al-4V/HAp composites. Results show that an optimal sintering time balances mechanical properties with bioactivity [51].

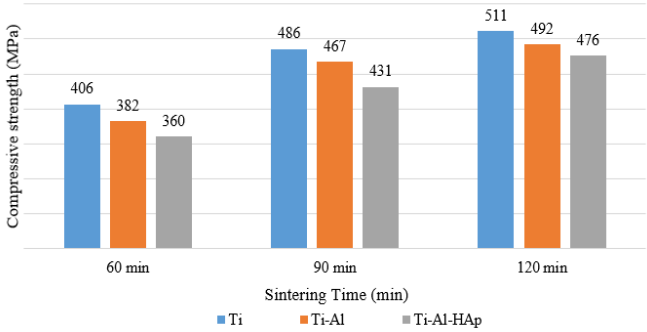

Figure 15. Compressive strength - sintering time chart

5.5 Micro-hardness test results

Figure 16 illustrates the micro-hardness test results as a function of sintering times. The measurements were conducted using a 4.9 N load with a dwell time of 15 seconds per sample. The results indicate a gradual increase in micro-hardness (HV) with increasing sintering time (60, 90, and 120 minutes). The micro-hardness continued to increase with longer sintering times, reaching its peak at 120 minutes for all compositions in group C (T_C = 379 HV, TA_C = 351 HV, and TAH_C = 298 HV). The observed increase in hardness is attributed to the enhanced densification at longer sintering times (1,300°C and 120 minutes), which reduces porosity and strengthens the material. Additionally, the variation in particle size during fabrication improved phase homogeneity and particle interactions, leading to increased resistance to deformation. Ti (Ti1 and Ti2), Al, and HAp particles contributed to this effect by minimizing crack propagation and enhancing material toughness. Furthermore, the addition of Al and HAp to Ti resulted in lower hardness [26, 52]. The Vickers hardness of Ti-6Al-4V typically ranges from 330 to 400 HV [53].

The standard deviation and standard error for the obtained results as shown in Tables 5-7.

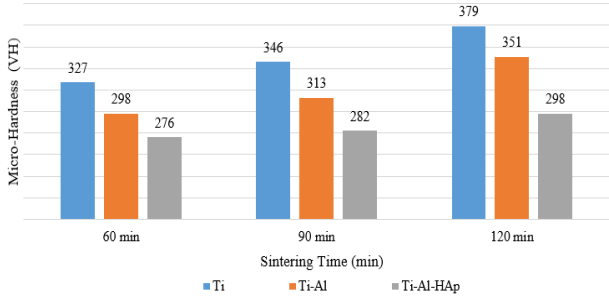

Figure 16. Microhardness -sintering time chart

Table 5. Statistical results of apparent density

Group	Sample	Std. Deviation	Std. Error
	T_A	0.0265	±0.57
A	TA_A	0.0165	±0.52
	TAH_A	0.0392	±0.51
	T_B	0.00896	±0.53
B	TA_B	0.0117	±0.48
	TAH_B	0.00711	±0.51
	T_C	0.02057	±0.38
C	TA_C	0.01143	±0.31
	TAH_C	0.00941	±0.3

Table 6. Statistical results of microhardness

Group	Sample	Std. deviation	Std. error
	T_A	0.54	±1.18
A	TA_A	1.47	±0.85
	TAH_A	1.87	±1.08
	T_B	2.54	±1.47
B	TA_B	1.85	±1.07
	TAH_B	1.34	±0.77
	T_C	0.57	±1.48
C	TA_C	1.07	±0.62
	TAH_C	1.02	±0.59

Table 7. Statistical results of compression.

Group	Sample	Std. deviation	Std. error
	T_A	3.86	±4.58
A	TA_A	4.55	±3.22
	TAH_A	6.68	±8.19
	T_B	6.16	±4.36
B	TA_B	6.21	±4.32
	TAH_B	3.73	±2.65
	T_C	5.29	±4.25
C	TA_C	2.95	±2.08
	TAH_C	3.74	±2.65

5.6 X-Ray diffraction (XRD) analyzing results

Figure 17 illustrates the XRD patterns obtained from the best-performing sample, TAH_C. The multiple peaks observed indicate the presence of various compounds resulting from the decomposition of hydrocarbons and their interaction with Ti and Al. The XRD analysis of TAH_C identified the following compounds: TiP_2O_7, Ti, Al_2Ti, $CaTiO_3$, TiO_2, $CaTi_4P_6O_{24}$, and $Na_2Ti_3O_7$, along with their respective standard cards. In the context of biomaterials, analyzing the presence of compounds such as TiP_2O_7, TiO_2, Al_2Ti, $Na_2Ti_3O_7$, $CaTi_4P_6O_{24}$, and

$CaTiO_3$ formed after sintering Ti with Al and hydroxyapatite (HAp) at high sintering time (120 minutes at 1,300°C) provides valuable insights into their potential effects on biocompatibility, mechanical properties, and stability. For example, $CaTiO_3$ has attracted interest for its bioactivity, especially in bone repair applications. It demonstrates compatibility with bone tissue and can promote apatite formation on its surface when exposed to bodily fluids, which is an indicator of bioactivity. Additionally, it has good chemical stability and hardness, which could contribute to mechanical integrity in load-bearing implants. The combination of Ca and Ti in $CaTiO_3$ can be beneficial in orthopedic implants and bone scaffolds, as calcium is crucial for bone cell signaling and formation, while Titanium Pyrophosphate (TiP_2O_7) has structural stability and wear resistance, but limited research on its specific interactions with biological systems exists. However, phosphate-based compounds promote osteoconductivity, potentially benefiting bone integration in implants or bone grafts. The presence of these ceramic compounds in sample TAH_C leads to no need for coating or additional processes that make the product more biocompatible [54-61].

5.7 Analysis results of energy dispersive X-ray spectroscopy (EDS)

Figure 18 illustrates the EDS analysis results of the best-performing sample TAH_C. This test was conducted to examine the effect of adding 2% HAp and 6% Al with Ti on the microstructure of the sample and their impact on other properties of Ti elements produced by P/M technology. The chemical surface analysis revealed significant peaks for titanium, aluminum, calcium, phosphorus, and oxygen, with a small amount of silicon from the raw materials. EDS examination showed that the sample TAH_C had high purity.

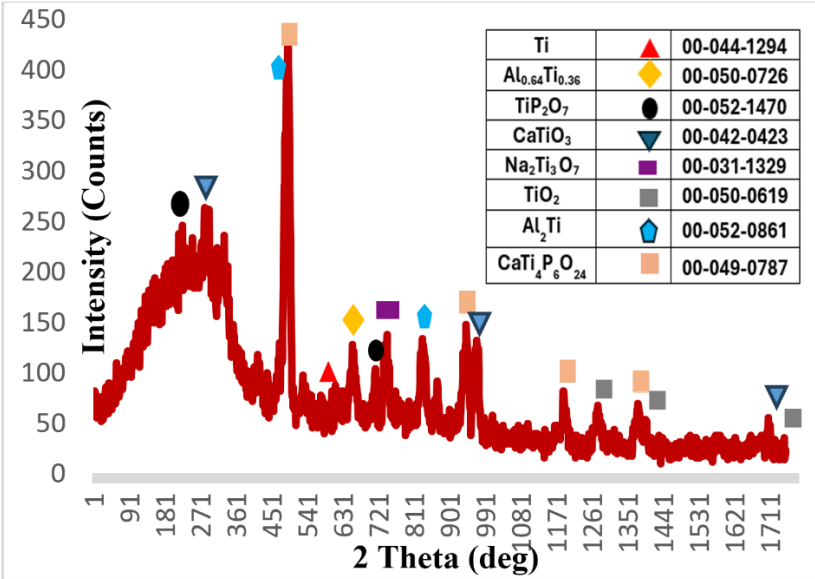

Figure 17. XRD patterns analysis results of the sample TAH_C

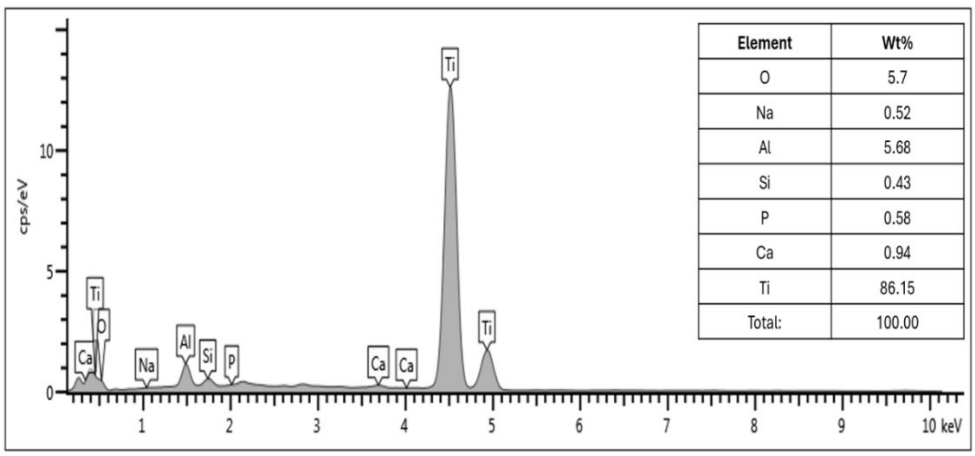

Figure 18. EDS analysis of the sample TAH_C

5.8 SEM analysis

Figure 19 shows the SEM examination conducted on the best-performing sample TAH_C. Observation is shown in Figure 13, displaying the sample mentioned above at 50 µm. The grains and pores in this figure exhibit varying sizes and dimensions, with particle (grain) sizes ranging from approximately 16 µm to 40 µm in TAH_C. SEM analysis revealed greater homogeneity in particle size distribution within the sample TAH_C, contributing to its higher sintering time (120 minutes at 1,300°C). The Gwyddion application was used to determine the Roughness Average (Ra) in nanometers (nm) for the sample TAH_C. Based on the SEM image of the sample, the surface roughness average of this sample (3D

image) was obtained. The Roughness Average R_a (nm) of the sample TAH_C is 137nm. This result was obtained because of the present nanoscale particle size in HAp (72nm) and Al (112nm), as well as being affected by higher sintering time [62]. The nanostructure material caused the implant surface to have a nano-roughness surface, with a nano-roughness surface, (less than 1 μm). The surface with this nano-roughness improves the adsorption of a protein and the cellular responses, leading to more and quicker, reliable osseointegration [63].

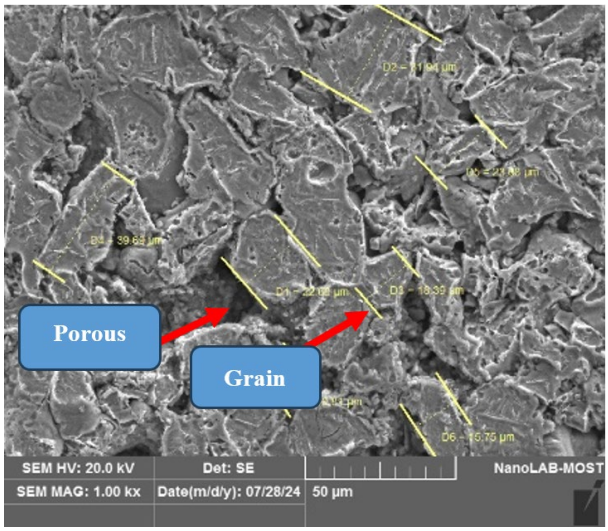

Figure 19. SEM image of sample TAH_C

5.9 Atomic Absorption Spectroscopy (AAS) analyzing results

This study measured the ion release from the best-performing sample TAH_C in Ringer's solution. After 14 days in Ringer's solution, the maximum Titanium ion release was 0.912 ppm from TAH_C, as shown in Figure 20. This result is consistent with previous studies, which have reported the ion release of titanium in biological solutions, where titanium ions are typically released in low concentrations due to corrosion or surface degradation [64]. After 14 days in Ringer's solution, the Aluminum ion release from the sample TAH_C was 0 ppm, as illustrated in Figure 14. This finding suggests minimal or no release of aluminum, which is consistent with the inert behavior of aluminum in the titanium-based alloys under the experimental conditions [65].

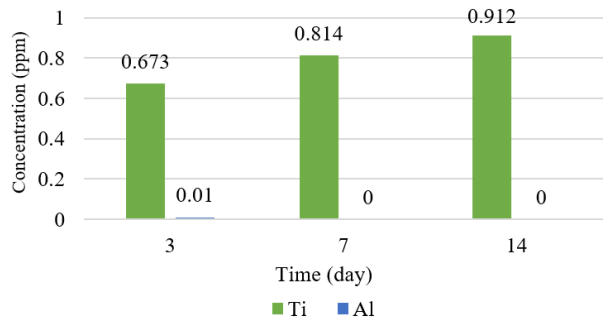

Figure 20. Atomic Absorption Spectroscopy analysis of sample TAH_C

Titanium, known for its non-toxicity, is naturally removed by the body and bonds well with bone. The titanium ion release is usually minimal due to its high biocompatibility, and the body can effectively handle and eliminate any excess titanium ions [66]. It has been shown that when titanium ions are released, they do not accumulate to toxic levels and are excreted without causing harm [67]. Furthermore, the ion release stabilizes after a period due to adsorption processes, with various responses occurring on the implant surface when interacting with bone [68]. Adsorption of metal ions is maintained by cell generation at the implant's surface, preventing further ion release and ensuring the material's long-term stability and biocompatibility [69].

5.10 MTT assay: Analyzing results

Formazan crystals, when dissolved, show absorbance at 500-600 nanometers, with a darker color indicating more viable cells. Materials like Titanium (Ti), Aluminum (Al), and Hydroxyapatite (HAp) used in bone fixation are evaluated for their impact on the human body. Titanium is known for its corrosion resistance, durability, and biocompatibility, forming a protective titanium oxide layer that makes it non-toxic [70]. Aluminum enhances the mechanical properties but poses toxicity risks when accumulated in the body, though proper coating minimizes this risk [71]. Hydroxyapatite, a natural bone component, is highly biocompatible and aids bone healing by enhancing the interaction between the implant and the surrounding bone tissue [72]. Ti-Al-HAp materials degrade slowly, releasing minimal ions, typically remaining within safe limits unless under excessive corrosion, making them safe with low toxicity when adhering to medical standards [73].

The best cell viability recorded was 86.7% for cells on a powder mix after three days. Hydroxyapatite aids in bone integration, offering excellent biological and mechanical properties. The MTT assay showed a 13.3% cytotoxicity rate after three days, indicating moderate biocompatibility, which is considered acceptable in initial evaluations, as shown in Figure 21. Titanium's interaction with tissues is minimal due to its inertness, while aluminum, linked to Alzheimer's disease over extended periods, dissolves more quickly in powder form, releasing trivalent aluminum ions [74]. Aluminum itself is a controversial material that is controversial for human exposure. The accumulation of aluminum in the body can be toxic, as increased levels have been associated with health risks such as neurotoxicity and kidney disease. In TiAlHap, aluminum is incorporated with titanium and hydroxyapatite to form an integrated material with enhanced mechanical and chemical properties. Toxicity concerns revolve around the potential release of aluminum ions into the body due to corrosion or degradation. However, when these materials are properly manufactured and coated, the risk of aluminum leakage is low, reducing the potential health hazards. Hydroxyapatite is a natural component of human bones and teeth, making it a highly biocompatible material. It does not cause significant immune reactions or toxicity in the body [75].

Powder metallurgy technology at 1,300°C transforms aluminum into a crystalline state, eliminating its toxicity long-term and addressing titanium's inertness. Adding hydroxyapatite improves the interaction between bone and fixation plates, enhancing osteointegration, reducing toxicity, and aiding in healing damaged bones [76]. The cytotoxicity of the tested material was evaluated using the MTT assay, following the ISO 10993-5 guidelines for in vitro cytotoxicity testing. This standard provides a framework for assessing the biological effects of medical device materials on cultured

mammalian cells. In this study, MG63 osteoblast-like cells were used to determine the viability and metabolic activity in response to the material extracts [77].

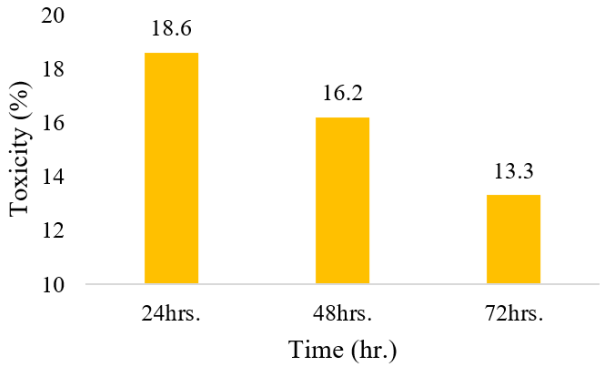

Figure 21. The toxicity of cell MG63 – time chart

6. CONCLUSION

This study employed two distinct particle sizes of pure Ti (Ti1 at 484.9 nm and Ti2 at 174.6 nm) and investigated three different chemical compositions (pure Ti, Ti-Al, and Ti-Al-HAp). The samples were fabricated using powder metallurgy techniques with varying sintering times. The research underscores the significant impact of sintering duration on the optimization of the physical, mechanical, and biological properties of titanium-based composites. Sintering durations of 60, 90, and 120 minutes at the same temperature of 1300°C resulted in significant improvements in the apparent density (3.49%), relative density (6.69%), and compressive strength (17.25%), while concurrently reducing relative porosity (2.41%) and microhardness (8.87%) in CP-Ti, Ti–6%Al, and Ti–6%Al–2%HAp composites. Furthermore, the incorporation of hydroxyapatite enhanced bioactivity, and the addition of aluminum contributed to better mechanical properties. X-ray diffraction (XRD) and scanning electron microscopy (SEM) analyses confirmed the formation of bioactive phases and favorable microstructural characteristics. Additionally, the MTT assay and Atomic Absorption Spectroscopy (AAS) results demonstrated the materials' biocompatibility and low ion release, with a reduction in toxicity by approximately 28.49%. These findings underscore the potential of sintering-optimized Ti-based composites as promising candidates for biomedical applications, particularly in load-bearing implants.

ACKNOWLEDGMENT

My supervisors: Prof. Dr. Niveen Jamal Abdulkader and Assistant. Prof. Dr. Laith Wadah, Prof. Dr. Kadum Kamel, all materials engineering department/ UOT staff, my family, and Mrs. Maysaloon Fakher (Iraqi writer).

AUTHORS' CONTRIBUTIONS

Marwa Hadi: Conceptualization, Methodology, Investigation, Writing—original draft. Niveen Jamal Abdulkader Investigation, Supervision, Resources, Project administration, writing review, and editing. Layth Al-Gebory: Conceptualization, Methodology, Investigation, Supervision, Resources, Project administration, writing review, and editing. All authors have read and approved the final manuscript.

REFERENCES

[1] Sridharan, R., Cameron, A.R., Kelly, D.J., Kearney, C.J., O'Brien, F.J. (2015). Biomaterial based modulation of macrophage polarization: A review and suggested design principles. Materials Today, 18(6): 313-325. https://doi.org/10.1016/j.mattod.2015.01.019

[2] Kiradzhiyska, D.D., Mantcheva, R.D. (2019). Overview of biocompatible materials and their use in medicine. Folia Medica, 61(1): 34-40. https://doi.org/10.2478/folmed-2018-0038

[3] Zaman, H.A., Sharif, S., Idris, M.H., Kamarudin, A. (2015). Metallic biomaterials for medical implant applications: A review. Applied Mechanics and Materials, 735: 19-25. https://doi.org/10.4028/www.scientific.net/amm.735.19

[4] Sarraf, M., Rezvani Ghomi, E., Alipour, S., Ramakrishna, S., Liana Sukiman, N. (2021). A state-of-the-art review of the fabrication and characteristics of titanium and its alloys for biomedical applications. Bio-design and Manufacturing, 5: 371-395. https://doi.org/10.1007/s42242-021-00170-3

[5] Shanmuganantha, L., Khan, M.U.A., Sulong, A.B., Ramli, M.I., Baharudin, A., Ariffin, H.M., Ng, M.H. (2022). Characterization of titanium ceramic composite for bone implants applications. Ceramics International, 48(16): 22808-22819. https://doi.org/10.1016/j.ceramint.2022.04.140

[6] Baltatu, M.S., Tugui, C.A., Perju, M.C., Benchea, M., Spataru, M.C., Sandu, A.V., Vizureanu, P. (2019). Biocompatible titanium alloys used in medical applications. Revista de Chimie, 70(4): 1302-1306.

[7] Kim, T., See, C.W., Li, X., Zhu, D. (2020). Orthopedic implants and devices for bone fractures and defects: Past, present and perspective. Engineered Regeneration, 1: 6-18. https://doi.org/10.1016/j.engreg.2020.05.003

[8] Khorasani, A.M., Goldberg, M., Doeven, E.H., Littlefair, G. (2015). Titanium in biomedical applications—properties and fabrication: A review. Journal of biomaterials and tissue engineering, 5(8): 593-619. https://doi.org/10.1166/jbt.2015.1361

[9] Liu, H.W., Bishop, D.P., Plucknett, K.P. (2015). A comparison of Ti–Ni and Ti-Sn binary alloys processed using powder metallurgy. Materials Science and Engineering: A, 644: 392-404. https://doi.org/10.1016/j.msea.2015.07.085

[10] Qu, J., Ma, X., Xie, H., Zhang, D., Song, Q., Yin, H. (2020). Mechanical and corrosion properties of porous titanium prepared by an electro-assisted powder metallurgy approach. JOM, 72: 4674-4681. https://doi.org/10.1007/s11837-020-04406-y

[11] Metal Powder Technology. Economic considerations for powder metallurgy structural parts. https://www.metal-powder.tech/introduction-to-powder-metallurgy/economic-considerations-for-powder-metallurgy-structural-parts/, accessed on Apr. 10, 2025.

[12] Danninger, H., Calderon, R.D.O., Gierl-Mayer, C. (2017). Powder metallurgy and sintered materials. Ullmann's Encyclopedia of Industrial Chemistry, 1-57. https://doi.org/10.1002/14356007.a22_105.pub2

[13] Wnek, G., Bowlin, G. (Eds.). (2008). Encyclopedia of Biomaterials and Biomedical Engineering (2nd ed.). CRC Press. https://doi.org/10.1201/9780429154065
[14] Rodriguez-Contreras, A., Punset, M., Calero, J.A., Gil, F.J., Ruperez, E., Manero, J.M. (2021). Powder metallurgy with space holder for porous titanium implants: A review. Journal of Materials Science & Technology, 76: 129-149. https://doi.org/10.1016/j.jmst.2020.11.005
[15] Reig, L., Tojal, C., Busquets, D.J., Amigó, V. (2013). Microstructure and mechanical behavior of porous Ti–6Al–4V processed by spherical powder sintering. Materials, 6(10): 4868-4878. https://doi.org/10.3390/ma6104868
[16] Azeez, A.A., Danyuo, Y., Obayemi, J.D. (2020). Effect of particle size and sintering time on the mechanical properties of porous Ti–6Al–4V implant. SN Applied Sciences, 2(5): 819. https://doi.org/10.1007/s42452-020-2637-z
[17] Ramli, M.I., Sulong, A.B., Muhamad, N., Muchtar, A., Arifin, A., Mohd Foudzi, F., Hammadi Al-Furjan, M.S. (2018). Effect of sintering parameters on physical and mechanical properties of powder injection moulded stainless steel-hydroxyapatite composite. PloS one, 13(10): e0206247.
[18] Thian, E.S., Huang, J., Best, S.M., Barber, Z.H., Bonfield, W. (2005). Magnetron co-sputtered silicon-containing hydroxyapatite thin films—An in vitro study. Biomaterials, 26(16): 2947-2956. https://doi.org/10.1016/j.biomaterials.2004.07.058
[19] Jacobs, T., De Geyter, N., Morent, R., Van Vlierberghe, S., Dubruel, P., Leys, C. (2011). Plasma modification of PET foils with different crystallinity. Surface and Coatings Technology, 205: S511-S515. https://doi.org/10.1016/j.surfcoat.2011.01.029
[20] Huang, S., Zhao, Q., Yang, Z., Lin, C., Zhao, Y., Yu, J. (2023). Strengthening effects of Al element on strength and impact toughness in titanium alloy. Journal of Materials Research and Technology, 26: 504-516. https://doi.org/10.1016/j.jmrt.2023.07.206
[21] Omidi, N., Jabbari, A.H., Sedighi, M. (2018). Mechanical and microstructural properties of titanium/hydroxyapatite functionally graded material fabricated by spark plasma sintering. Powder Metallurgy, 61(5): 417-427. https://doi.org/10.1080/00325899.2018.1535391
[22] Kobayashi, M., Nihonmatsu, S., Okawara, T., Onuki, H., Sakagami, H., Nakajima, H., Shimada, J. (2019). Adhesion and proliferation of osteoblastic cells on hydroxyapatite-dispersed Ti-based composite plate. In Vivo, 33(4): 1067-1079. https://doi.org/10.21873/invivo.11575
[23] Farrahnoor, A., Zuhailawati, H. (2021). Effects of hydroxyapatite addition on the bioactivity of Ti-Nb alloy matrix composite fabricated via powder metallurgy process. Materials Today Communications, 27: 102209. https://doi.org/10.1016/j.mtcomm.2021.102209
[24] Shanmuganantha, L., Khan, M.U.A., Sulong, A.B., Ramli, M.I., Baharudin, A., Ariffin, H.M., Ng, M.H. (2022). Characterization of titanium ceramic composite for bone implants applications. Ceramics International, 48(16): 22808-22819. https://doi.org/10.1016/j.ceramint.2022.04.140
[25] Arivazhagan, A., Mani, K., Kamarajan, B.P., AGS, S.A., Vijayaragavan, S., Riju, A.A., Rajeshkumar, G. (2025). Mechanical and biocompatibility studies on additively manufactured Ti6Al4V porous structures infiltrated with hydroxyapatite for implant applications. Journal of Alloys and Compounds, 1010: 177966. https://doi.org/10.1016/j.jallcom.2024.177966
[26] Sadlik, J., Kosińska, E., Bańkosz, M., Tomala, A., Bruzda, G., Jampilek, J., Sobczak-Kupiec, A. (2024). Gradient titanium alloy with bioactive hydroxyapatite porous structures for potential biomedical applications. Materials, 17(22): 5511. https://doi.org/10.3390/ma17225511
[27] Yaşar, H., Ekmekci, B. (2021). The effect of micro and nano hydroxyapatite powder on biocompatibility and surface integrity of Ti6Al4V (ELI) in powder mixed electrical discharge machining. Surface Topography: Metrology and Properties, 9(1): 015015. https://doi.org/10.1088/2051-672X/abdda2
[28] Bai, Y., Wagner, G., Williams, C. B. (2017). Effect of particle size distribution on powder packing and sintering in binder jetting additive manufacturing of metals. Journal of Manufacturing Science and Engineering, 139(8): 081019. https://doi.org/10.1115/1.4036640
[29] Total Materia. Principles of Powder Metallurgy. https://www.totalmateria.com/en-us/articles/principles-of-powder-metallurgy/, accessed on Apr. 10, 2025.
[30] KINTEK. (2024). Understanding isostatic pressing in powder metallurgy. https://ar.kindle-tech.com/articles/understanding-isostatic-pressing-in-powder-metallurgy.
[31] Qian, M., Schaffer, G.B., Bettles, C.J. (2010). Sintering of titanium and its alloys. Sintering of Advanced Materials, Woodhead Publishing Series in Metals and Surface Engineering, pp. 324-355. https://doi.org/10.1533/9781845699949.3.324
[32] ASTM B822–20. (2020). Standard test method for particle size distribution of metal powders and related compounds by light scattering. West Conshohocken, PA, USA. https://www.astm.org/b0822-20.html.
[33] Bolzoni, L., Ruiz-Navas, E.M., Gordo, E. (2016). Understanding the properties of low-cost iron-containing powder metallurgy titanium alloys. Materials & Design, 110: 317-323. https://doi.org/10.1016/j.matdes.2016.08.010
[34] Callister Jr, W.D., Rethwisch, D.G. (2020). Materials Science and Engineering: An Introduction. John Wiley & Sons.
[35] Melville, J., Mortensen, D. (2014). Atomic absorption spectroscopy of metal alloys. Instrumental Methods in Analytical Chemistry.
[36] ASTM E9-19. (2019). Standard test methods of compression testing of metallic materials at room temperature. West Conshohocken, PA, USA. https://www.astm.org/e0009-19.html.
[37] ASTM E18-22. (2022). Standard test methods for rockwell hardness of metallic materials. West Conshohocken, PA, USA. https://store.astm.org/e0018-22.html.
[38] El Sawy, A.A., Shaarawy, M.A. (2014). Evaluation of metal ion release from Ti6Al4V and Co-Cr-Mo casting alloys: In vivo and in vitro study. Journal of Prosthodontics, 23(2): 89-97. https://doi.org/10.1111/jopr.12067
[39] Wang, J.Z., You, M.L., Ding, Z.Q., Ye, W.B. (2019). A

review of emerging bone tissue engineering via PEG conjugated biodegradable amphiphilic copolymers. Materials Science and Engineering: C, 97: 1021-1035. https://doi.org/10.1016/j.msec.2019.01.057
[40] Patterson, B.R., Parkhe, V.D., Griffin, J.A. (1987). Effect of particle size distribution on sintering. Sintering'85, 43-51. https://doi.org/10.1007/978-1-4613-2851-3_4
[41] Veiga, C., Davim, J.P., Loureiro, A.J.R. (2012). Properties and applications of titanium alloys: A brief review. Reviews on Advanced Materials Science, 32(2): 133-148.
[42] Marin, E., Lanzutti, A. (2023). Biomedical applications of titanium alloys: A comprehensive review. Materials, 17(1): 114. https://doi.org/10.3390/ma17010114
[43] Becker, T.H., Dhansay, N.M. (2021). Influence of porosity on the fatigue life of laser powder bed fusion–produced Ti6Al4V. Material Design & Processing Communications, 3(1): e141. https://doi.org/10.1002/mdp2.141
[44] Alkentar, R., Kladovasilakis, N., Tzetzis, D., Mankovits, T. (2023). Effects of pore size parameters of titanium additively manufactured lattice structures on the osseointegration process in orthopedic applications: A comprehensive review. Crystals, 13(1): 113. https://doi.org/10.3390/cryst13010113
[45] Li, X., Yao, C., Shen, J., Zhu, S., Kong, Y., Yao, C., Zhou, Y., Xia, J. (2024). The impact of titanium hydroxyapatite doping on the mechanical and biological properties of photocured resin. Micromachines, 15(8): 1040. https://doi.org/10.3390/mi15081040
[46] Agarwal, K.M., Singhal, A., Kapoor, A., Bhatia, D. (2021). Simulated analysis of Ti-6Al-4V processed through equal channel angular pressing for biomedical applications. Materials Science for Energy Technologies, 4: 290-295. https://doi.org/10.1016/j.mset.2021.08.005
[47] Hoseinzadeh, S., Gordani, G., Tavoosi, M., Alhakeem, M.R.H., Al-Bahrani, M., Estarki, M.R.L. (2024). Effect of sintering temperature and time on the microstructure, density, phase, selected mechanical and tribological properties of Cf/Si3N4 composite fabricated by the spark plasma sintering. Arabian Journal of Chemistry, 17(1): 105378. https://doi.org/10.1016/j.arabjc.2023.105378
[48] Rocha, S.S.D., Adabo, G.L., Henriques, G.E.P., Nóbilo, M.A.D.A. (2006). Vickers hardness of cast commercially pure titanium and Ti-6Al-4V alloy submitted to heat treatments. Brazilian Dental Journal, 17: 126-129. https://doi.org/10.1590/S0103-64402006000200008
[49] AZO Materials. Titanium (Ti) - Properties, Applications. https://www.azom.com/properties.aspx?ArticleID=712, accessed on Apr. 10, 2025.
[50] AZO Materials. Titanium Alloys - Ti6Al4V Grade 5. https://www.azom.com/properties.aspx?ArticleID=1547, accessed on Apr. 10, 2025.
[51] do Nascimento, M.H.M., Ambrosio, F.N., Ferraraz, D.C., Windisch-Neto, H., et al. (2021). Sulforaphane-loaded hyaluronic acid-poloxamer hybrid hydrogel enhances cartilage protection in osteoarthritis models. Materials Science and Engineering: C, 128: 112345. https://doi.org/10.1016/j.msec.2021.112345
[52] Liu, Q., Chu, J., Xie, Y., Li, Z., Wu, F., Feng, D., Xie, D. (2025). Novel Si-MXene/PAPP hybrid system for high-performance flame-retardant polypropylene composites. Polymer Degradation and Stability, 239: 111376. https://doi.org/10.1016/j.polymdegradstab.2025.111376
[53] SGS. Ti 6Al 4V (grade 5) titanium alloy data sheet. https://kyocera-sgstool.co.uk/titanium-resources/titanium-information-everything-you-need-to-know/ti-6al-4v-grade-5-titanium-alloy-data-sheet/, accessed on Apr. 10, 2025.
[54] ScienceDirect. Titanium dioxide. https://www.sciencedirect.com/topics/agricultural-and-biological-sciences/titanium-dioxide, accessed on Apr. 10, 2025.
[55] Ma, J.C., Benci, J.E., Feist, T.P. (1994). Effects of processing on the mechanical properties and oxidation behavior of Al2Ti. MRS Online Proceedings Library (OPL), 364: 1303. https://doi.org/10.1557/PROC-364-1303
[56] Lucero, H.A., Kintsurashvili, E., Marketou, M.E., Gavras, H. (2010). Cell signaling, internalization, and nuclear localization of the angiotensin converting enzyme in smooth muscle and endothelial cells. Journal of Biological Chemistry, 285(8): 5555-5568.
[57] Jeong, J., Kim, J.H., Shim, J.H., Hwang, N.S., Heo, C.Y. (2019). Bioactive calcium phosphate materials and applications in bone regeneration. Biomaterials Research, 23(1): 4. https://doi.org/10.1186/s40824-018-0149-3
[58] Jabbar, S.A., Abdulkader, N.J., Ahmed, P.S. (2024). The investigation on properties of Ti-5Si and Ti-5Nb implant alloys coated by bioactive based composite coating. Materials Research Express, 11(3): 036520. https://doi.org/10.1088/2053-1591/ad280a
[59] Tuyen, N.T.T., Tuan, T.Q., Toan, L.V., Tam, L.T., Pham, V.H. (2024). Synthesis of up-conversion CaTiO3: Er3+ films on titanium by anodization and hydrothermal method for biomedical applications. Materials, 17(13): 3376. https://doi.org/10.3390/ma17133376
[60] Punj, S., Singh, J., Singh, K.J.C.I. (2021). Ceramic biomaterials: Properties, state of the art and future prospectives. Ceramics International, 47(20): 28059-28074. https://doi.org/10.1016/j.ceramint.2021.06.238
[61] Matos, G.R.M. (2021). Surface roughness of dental implant and osseointegration. Journal of Maxillofacial and Oral Surgery, 20: 1-4. https://doi.org/10.1007/s12663-020-01437-5
[62] Chauhan, A.S., Maria, A., Managutti, A. (2015). Efficacy of simvastatin in bone regeneration after surgical removal of mandibular third molars: A clinical pilot study. Journal of Maxillofacial and Oral Surgery, 14: 578-585. https://doi.org/10.1007/s12663-014-0697-6
[63] Senopati, G., Rahman Rashid, R.A., Kartika, I., Palanisamy, S. (2023). Recent development of low-cost β-Ti alloys for biomedical applications: A review. Metals, 13(2): 194. https://doi.org/10.3390/met13020194
[64] Bowers, D.T., Olingy, C.E., Chhabra, P., Langman, L., et al. (2018). An engineered macroencapsulation membrane releasing FTY720 to precondition pancreatic islet transplantation. Journal of Biomedical Materials Research Part B: Applied Biomaterials, 106(2): 555-568. https://doi.org/10.1002/jbm.b.33862
[65] Vargas-Becerril, N., Reyes-Gasga, J., García-García, R. (2019). Evaluation of crystalline indexes obtained through infrared spectroscopy and x-ray diffraction in thermally treated human tooth samples. Materials Science and Engineering: C, 97: 644-649. https://doi.org/10.1016/j.msec.2018.12.081
[66] Jung, H.D. (2021). Titanium and its alloys for biomedical applications. Metals, 11(12): 1945.

https://doi.org/10.3390/met11121945
[67] Weng, L., Rostamzadeh, P., Nooryshokry, N., Le, H.C., Golzarian, J. (2013). In vitro and in vivo evaluation of biodegradable embolic microspheres with tunable anticancer drug release. Acta biomaterialia, 9(6): 6823-6833. https://doi.org/10.1016/j.actbio.2013.02.017
[68] Arregui, M., Latour, F., Gil, F.J., Pérez, R.A., Giner-Tarrida, L., Delgado, L.M. (2021). Ion release from dental implants, prosthetic abutments and crowns under physiological and acidic conditions. Coatings, 11(1): 98. https://doi.org/10.3390/coatings11010098
[69] Boukhvalov, D.W., Korotin, D.M., Efremov, A.V., Kurmaev, E.Z., Borchers, C., Zhidkov, I.S., Gunderov, D.V., Valiev, R.Z., Gavrilov, N.V., Cholakh, S.O. (2015). Modification of titanium and titanium dioxide surfaces by ion implantation: Combined XPS and DFT study. Physica Status Solidi (B), 252(4): 748-754. https://doi.org/10.1002/pssb.201451362
[70] Development and characterization of hydroxyapatite/β-TCP/chitosan composites for tissue engineering applications. Materials Science and Engineering: C, 56: 481-493. https://doi.org/10.1016/j.msec.2015.07.004
[71] Gadenne, V., Lebrun, L., Jouenne, T., Thebault, P. (2015). Role of molecular properties of ulvans on their ability to elaborate antiadhesive surfaces. Journal of Biomedical Materials Research Part A, 103(3): 1021-1028. https://doi.org/10.1002/jbm.a.35245
[72] Shi, H., Zhou, Z., Li, W., Fan, Y., Li, Z., Wei, J. (2021). Hydroxyapatite based materials for bone tissue engineering: A brief and comprehensive introduction. Crystals, 11(2): 149. https://doi.org/10.3390/cryst11020149
[73] Gong, W., Cheng, T., Liu, Q., Xiao, Q., Li, J. (2018). Surgical repair of abdominal wall defect with biomimetic nano/microfibrous hybrid scaffold. Materials Science and Engineering: C, 93: 828-837. https://doi.org/10.1016/j.msec.2018.08.053
[74] Bahraminasab, M., Talebi, A., Doostmohammadi, N., Arab, S., Ghanbari, A., Zarbakhsh, S. (2022). The healing of bone defects by cell-free and stem cell-seeded 3D-printed PLA tissue-engineered scaffolds. Journal of Orthopaedic Surgery and Research, 17(1): 320. https://doi.org/10.1186/s13018-022-03213-2
[75] Das, R., Bandyopadhyay, R., Pramanik, P. (2018). Carbon quantum dots from natural resource: A review. Materials today chemistry, 8: 96-109. https://doi.org/10.1016/j.mtchem.2018.03.003
[76] Zheng, X., Zhang, X., Wang, Y., Liu, Y., et al. (2021). Hypoxia-mimicking 3D bioglass-nanoclay scaffolds promote endogenous bone regeneration. Bioactive Materials, 6(10): 3485-3495. https://doi.org/10.1016/j.bioactmat.2021.03.011
[77] TheraIndx Lifesciences. Understanding the MTT assay for cytotoxicity testing of medical devices. https://www.theraindx.com/mtt-assay-a-vital-tool-for-testing-medical-device-safety.php, accessed on Apr. 10, 2025.